This article has been accepted for publication in a future issue of this journal, but has not been fully edited. Content may change prior to final publication. Citation information: DOI 10.1109/TIM.2019.2950578, IEEE Transactions on Instrumentation and Measurement

Vector Tracking Loop-Based GNSS NLOS Detection and Correction: Algorithm Design and Performance Analysis

Bing Xu, Qiongqiong Jia, and Li-Ta Hsu, *Member, IEEE*

***Abstract*—This paper deals with the non-line-of-sight (NLOS) reception issue in the field of global navigation satellite system (GNSS). The NLOS reception has attracted a significant amount of attention because it is one of the main factors that limit the GNSS position accuracy in urban areas. In this work, we dig into the baseband signal processing level to explore a new solution to the NLOS detection and correction by means of the vector tracking loop (VTL). The NLOS effects on both conventional scalar tracking loops (STL) and VTL are derived mathematically. Based on this, an NLOS detection algorithm is developed using metrics such as the equivalent noise bandwidth, the time delay of multi-correlator peaks, as well as code discriminator outputs. Once detected, the NLOS-induced measurement error is corrected before being fed forward into the navigation estimator to improve the position accuracy. Two field tests in urban areas in Hong Kong are conducted to illustrate the effectiveness of the proposed method in real applications. The NLOS correction performance is also assessed using simulated NLOS receptions with controllable time delays and reflection coefficients, which reveals how the proposed algorithm performs in different NLOS scenarios.**

***Index Terms*—Global navigation satellite system (GNSS), non-line-of-sight (NLOS) reception, vector tracking loops (VTL), software-defined receivers (SDR), urban canyon**

I. Introduction

GLOBAL navigation satellite system (GNSS) has been extensively used in various applications including the instrumentation and measurement systems such as phasor measurement in electric distribution systems [1], telecommunications and informatics systems in vehicular application [2], and navigator in intelligent transportation systems [3]. The urban canyon, characterized by narrow streets and tall buildings, is one of the most challenging environments for a device equipped with GNSS receiver. An abundance of literature in the field of GNSS has been aimed at the accuracy improvement in urban canyons [4-8]. In such challenging environments, the line-of-sight (LOS) GNSS signal is easily blocked, and its reflected version can be received by the receiver antenna. This phenomenon is called the non-line-of-sight (NLOS) reception, which is the research object of this work.

Intuitively, the additional route that the NLOS signal transmits introduces a longer pseudorange measurement, and consequently a position deviation [9]. From the perspective of ranging using pseudo-random-noise (PRN) codes (e.g., the global positioning system (GPS) L1 C/A code), the distance between the satellite and the receiver is obtained by finding the propagation delay of the auto-correlation function (ACF) peak. The conventional delay lock loop (DLL) keeps equivalent outputs in the symmetrical early and late correlators. This working mechanism results in that the DLL will lock onto the NLOS signal continuously, therefore resulting in an extra propagation delay estimation. The ACF of NLOS reception in a conventional DLL-based receiver differs from that of LOS signals only in its magnitude, considering the reflection attenuation. Therefore, anti-multipath techniques that exploit the characteristic of the distorted ACF are not applicable to the NLOS reception issue [10].

Techniques that deal with the NLOS reception issue can be divided into three categories, as summarized in Table I with related literatures.

TABLE I
TECHNIQUES DEALING WITH NLOS RECEPTION

Category	Techniques
Mitigation	Antenna design, e.g., choke-ring antenna[11]
	Consistency checking, e.g., the technique based on pseudorange residual and navigation solution [12-14]
	Kalman filter innovation-based detection [15]
Detection	Hardware-based techniques, e.g., array antenna [16], dual-polarization antenna [17], sky-pointing camera [18, 19]
	Machine learning techniques [20-23]
	3D building model [20, 24-27]
	Vector tracking loops (VTL) [28]
Correction	3D mapping-aided (3DMA) GNSS [24, 29], building height aided 3D light detection and ranging (3D LiDAR) [30], NLOS modeling [31]

The first category is mitigation, where any potentially contaminated measurements, including the NLOS reception,

B. Xu, Q. Jia and L.T. Hsu, are with Hong Kong Polytechnic University, Hong Kong, China (e-mail: pbing.xu@polyu.edu.hk; qiongjiawei@163.com; lt.hsu@polyu.edu.hk). Q. Jia is also with Civil Aviation University. This research was supported by the Hong Kong PolyU startup fund on the project 1-ZVKZ, "Navigation for Autonomous Driving Vehicle using Sensor Integration".

are directly removed or down-weighted without being clearly classified. A typical example of this method is the usage of choke-ring antenna [11], which gives low gains to satellites with low elevation angles. Compared to the antenna design, a more convenient and less expensive solution is the consistency checking [12-14]. The basic principle behind this technique is that NLOS measurements produce a less consistent pseudorange residual or navigation solution. Similar to the concept of receiver autonomous integrity monitoring (RAIM), the consistency checking fails in GNSS-challenging environments where a large proportion of the signals are NLOS-contaminated [14]. Another similar technique used in a Kalman filter-based estimation algorithm is that the NLOS reception is mitigated by comparing the innovations, i.e., the new measurements against predicted values based on the time-propagated navigation solution [15].

The second group is the NLOS reception detection, which tends to classify the received signals into different signal types, i.e., LOS/NLOS or/and multipath signal. One way of using the signal type classification is simply discarding the faulty measurements [27], which, however, may reduce satellite availability in deep urban areas. Another usage of the classification result is the well-known shadow matching algorithm [32]. Different from the conventional ranging based GNSS positioning, the shadow matching estimates the user position by comparing the measured and predicted satellite visibility with the aid of 3D building models. Various kinds of methods of distinguishing signal types are proposed. The hardware-based techniques include the assistance of dual-polarization antenna [17], sky-pointing camera [18, 19], etc. Machine learning technique has also been applied to classify signal types using features extracted from basic GNSS observables like satellite elevation angle and carrier-to-noise ratio [21, 23], and even at baseband signal processing level as reported in [22]. With the help of 3D building models, it is straightforward to determine the satellite visibility. In our previous work [28, 33], we proposed an innovative method of detecting the NLOS reception using the VTL. The preliminary experiments show encouraging results of this method. However, there's a lack of comprehensive and theoretical analysis on the principle behind this technique.

The third group is the NLOS-induced error correction. This kind of technique tries to use the NLOS path delay constructively. Range-based 3D mapping-aided GNSS positioning is a good example, where possible signal transmission routes including the reflected ones, are traced based on 3D building models [29]. This method provides an opportunity of obtaining the additional path delay of the reflected signal. Hence, the pseudorange bias can be corrected in the positioning stage. However, the high processing load is a great challenge for this method being applied to low-cost receivers. A novel 3D LiDAR-based method aided by building height information is proposed to detect and correct the NLOS-induced measurement error without the usage of ray-tracing techinique [30]. In [31], the NLOS-induced path delay is modeled as a function of elevation angle and the distance between the receiver and the building that reflects the NLOS signal. With this model, the NLOS-caused pseudorange measurement error can be corrected to avoid distorting the distribution of satellites and improve the position accuracy. However, this method still uses the ray-tracing algorithm which is computationally expensive.

In this paper, we dig into the baseband signal processing level to explore a new solution to the detection and correction of NLOS reception using VTL based on our previous work [28, 33], where preliminary experimental results have shown the effectiveness of this method. We extend the work by revealing the NLOS effect in the VTL mathematically, designing a reliable NLOS detection algorithm, and providing a quantitative performance assessment of this method.

Different from the conventional scalar tracking loop (STL)-based receiver, a VTL-based receiver jointly tracks all satellites via the navigation solution estimator, e.g., the commonly used extended Kalman filter (EKF). Benefitting from the interaction between different channels, the vector tracking loop shows superiority over the scalar tracking loop in terms of weak signal tracking [34, 35], immunity to interference and jamming [36, 37], dynamics tolerance [34], and the ability to bridge short signal outages [38]. In addition, the VTL for multipath studies has also been attempted in existing literatures such as our previous work [28, 39], and the ones [40-43]. A basic idea of these approaches is that the STL and VTL have different ACF outputs for the compound signal containing multipath due to the different tracking strategies; various measures can then be carried out using the ACF outputs and/or the corresponding code discriminator outputs. For example, in [28], measurement noise variance of the EKF is automatically increased for large discriminator values caused by multipath, thus down-weighting the multipath-contaminated measurements. In [40, 41], multipath-induced tracking errors for the VTL is theoretically derived and analyzed, showing the change of signal power on the in-phase arm and/or the quadrature arm of the Early and Late correlation outputs due to the presence of multipath. A new multipath detection technique is, therefore, proposed based on the in-phase and quadrature correlation values of the VTL via the technique of binary hypothesis test [42]. In [43], the multipath is classified as coherent and non-coherent multipath, with coherent multipath detected via the hypothesis test of the code discriminator output, and non-coherent multipath monitored based on outputs of the fast Fourier transform (FFT)-based frequency discriminator, which is feasible to dynamic applications such as vehicular navigation. Unlike these researches, however, this paper explores the application of VTL to the NLOS reception. Due to the absence of direct signal, NLOS reception impacts the correlation process in a different way from the multipath. By exploring the VTL architecture, this paper proposes not only to detect the NLOS occurrence, but also to correct the NLOS-induced error before being used for the navigation solution solving. The rationale behind this approach is that, the VTL closes the tracking loop using the navigation solution instead of the code tracking error, i.e., the code discriminator output. In another word, the VTL would not lock onto the NLOS signal given an accurate navigation solution using other healthy satellites and the receiver's

dynamics model. Therefore, the phase difference between the incoming NLOS signal and the local replica code would appear and remain during the NLOS reception period, which provides an opportunity of not only detecting the NLOS reception but also correcting the NLOS-induced error. To this end, we introduced new metrics such as the equivalent noise bandwidth of VTL, the time delay of multi-correlator peaks as well as code discriminator outputs to jointly detect the NLOS signal via a completed algorithm. Once detected, the NLOS-induced measurement error is corrected before being fed forward into the navigation estimator to improve the position accuracy.

Compared to the techniques listed in Table I, the NLOS detection and correction based on the advanced vector tracking loop can enhance the quality of measurements of GNSS-capable instruments in urban environment without any external aiding of instrumentation or software, which represents the main contribution of this paper.

The remainder of the paper is organized as follows. Section II provides the methodology used in this paper, including the NLOS signal model and the proposed vector tracking loop-based NLOS detection and correction algorithm. In section III, the proposed algorithm is assessed in two field tests, with results analyzed from various perspectives. This section also gives the performance analysis using simulated NLOS reception with controllable parameters. Section IV concludes the paper.

II. METHODOLOGY

In this section, we introduce the methodology used in this paper. Intermediate frequency (IF) NLOS signal model is analyzed first with a focus on its effect on code tracking in conventional scalar tracking loops. Subsequently, the proposed vector tracking loop-based NLOS detection and correction algorithm will be given, before which the vector tracking loop design and modelling, the VTL's response to NLOS reception in terms of code auto-correlation function, and the concept of equivalent noise bandwidth of VTL are described in detail.

A. Signal Model

In this paper, we use the GPS L1 C/A signal for analysis. The proposed method can be applied to other GNSS signals with proper modification. Assuming there's no navigation bit transition in one coherent integration time interval, after the front-end filtering, down-conversion to intermediate frequency and sampling, the digitized GPS IF signal containing single NLOS reception is modeled as

$$\begin{aligned} y(i) = & \sum_{m=1,m\neq j}^{M} \left(A^m C^m \left(i-\tau^m \right) \cos\left(2\pi \left(f_{IF}^m + f_d^m \right) i + \varphi^m \right) \right) \\ & + \alpha^{\mathrm{NLOS}} A^j C^j \left(i-\tau^{\mathrm{LOS},j} - \tau^{\mathrm{NLOS}} \right) \cos\left(2\pi \left(f_{IF}^j + f_d^j \right) i + \varphi^j \right) \\ & + e(i) \end{aligned} \tag{1}$$

where $y(i)$ is the IF signal sampled at time $t = i \cdot T_s$; T_s is the sampling time interval in seconds; A^m is the signal amplitude of the m-th satellite; $C(\cdot)$ is the PRN code; τ^m is the PRN code delay; f_{IF} and φ are the frequency and initial phase of the IF carrier in hertz and radians, respectively; f_d is the Doppler frequency in hertz; j is the NLOS satellite index; Superscripts "NLOS" and "LOS" denote the NLOS and LOS-related parameters, respectively; α^{NLOS} is the NLOS reflection coefficient; τ^{NLOS} is the additional code delay of the NLOS reception relative to the assumed LOS signal, and $e(i)$ is the additive band-limited white Gaussian noise.

The NLOS effect on the code is much severer than that on the carrier. Therefore, in the following analysis, we assume that the local carrier replica is perfectly aligned with the carrier in the incoming signal. In a typical GPS receiver, three code replicas, referred to as the early (E), prompt (P), and late (L) code replicas, with a spacing of $d/2$ chip (d is the correlator spacing between the Early and the Late code), are created to correlate with the incoming code. The correlator outputs are integrated and dumped over one coherent integration time interval. Ignoring the noise, final correlator outputs will be generated as

$$\begin{aligned} E(n) &= \begin{cases} A^m \cdot R\left(\tau_e^m + d/2 \right) & \text{LOS} \\ \alpha^{\mathrm{NLOS}} A^j \cdot R\left(\tau_e^{\mathrm{NLOS}} + d/2 \right) & \text{NLOS} \end{cases} \\ P(n) &= \begin{cases} A^m \cdot R\left(\tau_e^m \right) & \text{LOS} \\ \alpha^{\mathrm{NLOS}} A^j \cdot R\left(\tau_e^{\mathrm{NLOS}} \right) & \text{NLOS} \end{cases} \\ L(n) &= \begin{cases} A^m \cdot R\left(\tau_e^m - d/2 \right) & \text{LOS} \\ \alpha^{\mathrm{NLOS}} A^j \cdot R\left(\tau_e^{\mathrm{NLOS}} - d/2 \right) & \text{NLOS} \end{cases} \end{aligned} \tag{2}$$

where $R(\cdot)$ is the auto-correlation function of the PRN code given in Appendix I. $\tau_e^m = \bar{\tau}^m - \tau^m$ and $\tau_e^{\mathrm{NLOS}} = \bar{\tau}^{\mathrm{NLOS}} - \left(\tau^{\mathrm{LOS},j} + \tau^{\mathrm{NLOS}} \right)$ are code phase differences between the local code replica and the received code for LOS and NLOS satellites, respectively, with $\bar{\tau}^m$ and $\bar{\tau}^{\mathrm{NLOS}}$ the corresponding estimated code delays. The output of the code discriminator, normalized noncoherent early minus late envelope [44] , is (see Appendix I for detailed derivation)

$$\begin{aligned} \Delta\tau(n) &= \frac{1}{2} \frac{E(n) - L(n)}{E(n) + L(n)} \\ &= \frac{1}{2} \frac{R\left(\tau_e + d/2 \right) - R\left(\tau_e - d/2 \right)}{R\left(\tau_e + d/2 \right) + R\left(\tau_e - d/2 \right)} \\ &= -\frac{\tau_e}{T_C}, \quad -\frac{T_C}{2} \le \tau_e \le \frac{T_C}{2}. \end{aligned} \tag{3}$$

where T_C is the chip duration, τ_e the code phase difference between local code replica and the received code.

In the conventional STL-based receiver, the code tracking error, namely the code discriminator output, is filtered and fed back to the code numerical controlled oscillator (NCO) to adjust the phase of the local code replica, leading to equal outputs in

This article has been accepted for publication in a future issue of this journal, but has not been fully edited. Content may change prior to final publication. Citation information: DOI 10.1109/TIM.2019.2950578, IEEE Transactions on Instrumentation and Measurement

the Early and Late correlators. In this way, both τ_e^m and τ_e^{NLOS} fluctuate around zeros, and the estimated code delay for LOS and NLOS satellites are approximately τ^m and $\left(\tau^{\mathrm{LOS},j}+\tau^{\mathrm{NLOS}}\right)$, respectively. Therefore, the NLOS-induced pseudorange measurement error is τ^{NLOS} in chips and is theoretically unlimited.

In addition, the ACF of NLOS reception in a conventional DLL-based receiver differs from that of LOS signals only in its magnitude. Hence, it's difficult for the STL to distinguish between LOS and NLOS signals from the perspective of the ACF shape. To solve this problem, we use the advanced GNSS signal tracking architecture, vector tracking loop, which is introduced in the next section.

B. Proposed Method of NLOS Detection and Correction

In this part, we present the proposed method of NLOS detection and correction. The system-level block diagram of the proposed method is shown in Fig. 1. GPS IF signal file is input to the vector tracking loop-based software-defined receiver (SDR). Code discriminator output and multi-correlator outputs are used for NLOS detection and correction. If detected, the NLOS-induced error correction will be input to the EKF for user position, velocity and time (PVT) estimation. Details of proposed method are given in the following subsections.

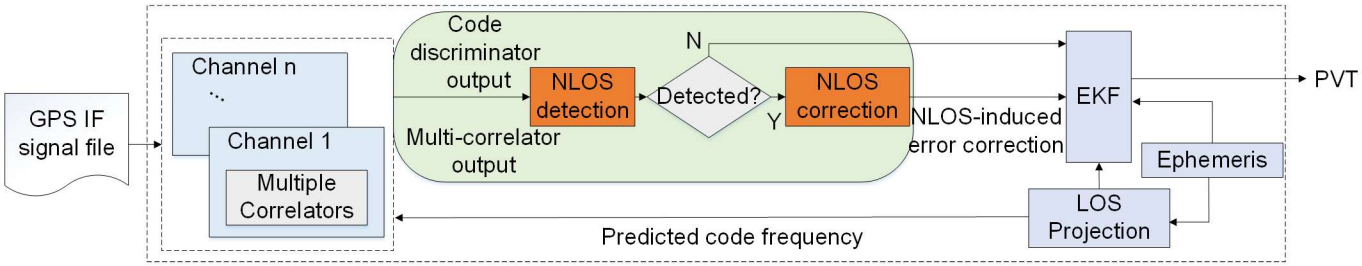

Fig. 1. System-level block diagram of the proposed method of NLOS detection and correction.

1) Vector Tracking Loop Design and Modelling

In conventional GPS receivers, each acquired satellite is allocated to an individual tracking channel. Each channel has two closed loops, one for code and one for carrier. The VTL-based receiver designed in this paper is shown in Fig. 2, where the carrier is still tracked using the conventional phase lock loop, while the code is tracked in the vector mode.

As shown in Fig. 2, in each channel, IF signals are first multiplied with locally generated carrier replica in both in-phase and quadrature arms. Correlation is then performed between the code replicas and the received ones. Afterwards, correlation results are integrated and dumped (I&D). The output of these integrations is used as the input to the carrier/code loop discriminator to find the phase error of the local carrier and code replicas. In each carrier loop, the carrier discriminator output is filtered and fed back to the carrier NCO. For the code tracking loop, code discriminator outputs of all channels are forwarded into the navigation processor for estimating the navigation solution. In this paper, the EKF is used. The output of the carrier loop filter, i.e., Doppler shift frequency, is also fed into the EKF to help estimate the user velocity and clock drift.

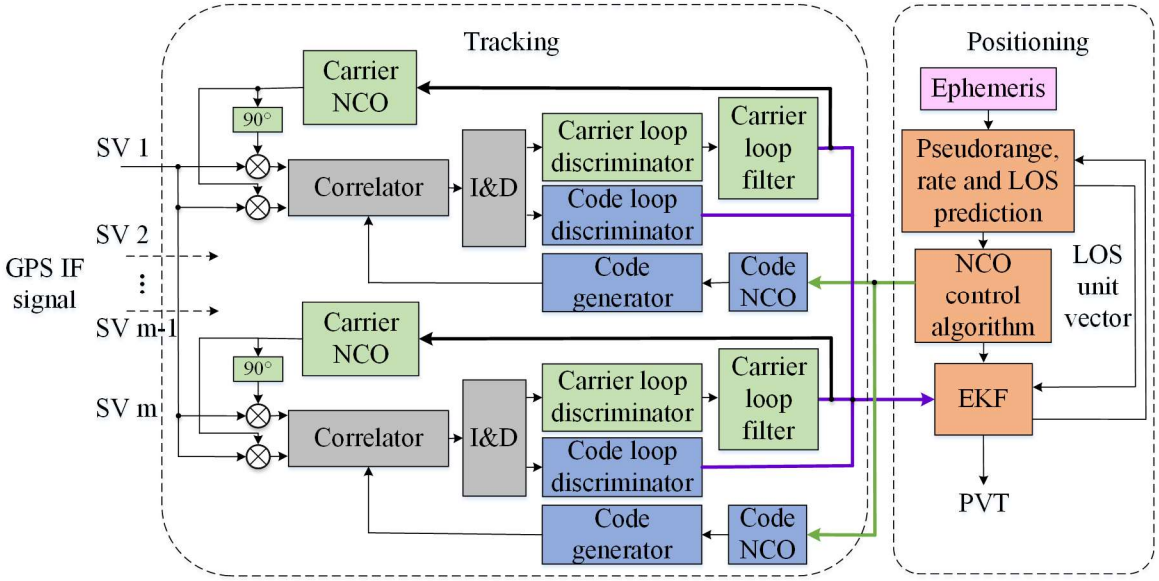

Fig. 2. The architecture of the proposed VTL.

The EKF estimates the navigation solution based on its system propagation and the measurements, which is described

in detail in Appendix II. After obtaining the navigation solution, the pseudorange and its rate and the LOS vector between the receiver and the satellites are predicted using the satellite ephemeris data. Finally, the predicted pseudorange is used to control the code NCO frequency, which is fed back to close each channel. The local code replica frequency at epoch k is given by

$$f_{code,k}^{m} = f_{CA} \times \left(1 - \frac{\hat{\rho}_k^m - \hat{\rho}_{k-1}^m}{c \cdot T_0}\right) \tag{4}$$

$$\hat{\rho}_k^m = \left\| \mathbf{p}_k - \mathbf{p}_k^m \right\| + \delta\hat{\rho}_{sv,c}^m + \delta\hat{\rho}_I^m + \delta\hat{\rho}_T^m - \delta b_k \tag{5}$$

where $\hat{\rho}_k^m$ is the predicted pseudorange at epoch k; $\mathbf{p}_k$ and $\mathbf{p}_k^m$ are the predicted receiver position and the satellite position at epoch k, respectively. $\delta\hat{\rho}_{sv,c}^m$, $\delta\hat{\rho}_I^m$, $\delta\hat{\rho}_T^m$ and δb_k are pseudorange error corrections in meters due to satellite clock error, ionospheric and tropospheric delay, user clock error, respectively; f_{CA} is the nominal code chipping rate; c is the speed of light, and T_0 is the EKF update interval.

2) NLOS Effects on Vector Tracking Loop

In this part, we present the response to NLOS reception in the VTL and show the basic principle of using VTL to detect and correct NLOS reception. We have derived that the estimated code delay for the NLOS reception in the STL is the code delay of the blocked LOS signal plus the additional code delay of the NLOS reception, i.e., $\left(\tau^{\mathrm{LOS},j} + \tau^{\mathrm{NLOS}}\right)$. In other words, the pseudorange measurement error is $\tau^{\mathrm{NLOS}} \times c / f_{CA}$ in meters. We will show VTL's response to NLOS reception, based on which an effective NLOS detection and correction algorithm will be proposed.

To begin with, we rewrite (A24) in Appendix II, namely the update of the EKF state vector, $\delta\mathbf{x}_k$, in case of the occurrence of NLOS reception at epoch k, as

$$\begin{aligned} \delta\mathbf{x}_k^{\mathrm{NLOS}} &= \delta\mathbf{x}_{k|k-1} + \mathbf{G}_k^{\mathrm{NLOS}} \boldsymbol{\gamma}_k^{\mathrm{NLOS}} \\ &= \delta\mathbf{x}_{k|k-1} + \mathbf{G}_k^{\mathrm{NLOS}} \left(\delta\mathbf{z}_k^{\mathrm{NLOS}} - \mathbf{H}_k \delta\mathbf{x}_{k|k-1}\right) \end{aligned} \tag{6}$$

where $\mathbf{G}_k^{\mathrm{NLOS}}$ is the Kalman filter gain during the NLOS reception period; $\boldsymbol{\gamma}_k^{\mathrm{NLOS}} = \delta\mathbf{z}_k^{\mathrm{NLOS}} - \mathbf{H}_k \delta\mathbf{x}_{k|k-1}$ is measurement innovation, where $\delta\mathbf{z}_k^{\mathrm{NLOS}}$ is the measurements when NLOS reception occurs, and $\mathbf{H}_k$ is the measurement matrix given in the Appendix II. In the absence of NLOS reception, with an optimal Kalman gain, the measurement innovation sequence can be considered as a white noise sequence. When the NLOS reception occurs, the predicted error state $\mathbf{H}_k \delta\mathbf{x}_{k|k-1}$ retains almost unchanged given an accurate estimated position using other healthy satellites and the user dynamics model. As a result, the measurement innovation sequence would deviate from the zeros, which provides an opportunity for detecting the NLOS reception.

From the perspective of signal tracking, the replica code phase would always be aligned with direct signal, although it is blocked in the case of NLOS reception. Hence, the estimated code replica phase in VTL should ideally be the code delay of the blocked LOS signal, i.e., $\bar{\tau}^{\mathrm{NLOS}} = \tau^{\mathrm{LOS},j}$. Therefore, the code discriminator output for NLOS becomes

$$\begin{aligned} \Delta\tau^{\mathrm{NLOS}}(n) &= \frac{1}{2} \frac{E^{\mathrm{NLOS}}(n) - L^{\mathrm{NLOS}}(n)}{E^{\mathrm{NLOS}}(n) + L^{\mathrm{NLOS}}(n)} \\ &= \frac{1}{2} \frac{\begin{pmatrix} R\left(\bar{\tau}^{\mathrm{NLOS}} - \left(\tau^{\mathrm{LOS},j} + \tau^{\mathrm{NLOS}}\right) + d/2\right) - \\ R\left(\bar{\tau}^{\mathrm{NLOS}} - \left(\tau^{\mathrm{LOS},j} + \tau^{\mathrm{NLOS}}\right) - d/2\right) \end{pmatrix}}{\begin{pmatrix} R\left(\bar{\tau}^{\mathrm{NLOS}} - \left(\tau^{\mathrm{LOS},j} + \tau^{\mathrm{NLOS}}\right) + d/2\right) + \\ R\left(\bar{\tau}^{\mathrm{NLOS}} - \left(\tau^{\mathrm{LOS},j} + \tau^{\mathrm{NLOS}}\right) - d/2\right) \end{pmatrix}} \\ &= -\frac{\tau^{\mathrm{NLOS}}}{T_C}, 0 \le \tau^{\mathrm{NLOS}} \le \frac{T_C}{2}. \end{aligned} \tag{7}$$

Note that in (7), $\tau^{\mathrm{NLOS}} \ge 0$ is due to the fact the NLOS reception has a longer path delay than the direct signal. Fig. 3 illustrates this process. The code delay of the NLOS reception manifests itself as the code tracking error in the VTL, which can also be used to detect and correct the NLOS-induced error. For comparison, we also show the ACF in the STL.

However, as suggested in (6), the navigation solution is still affected by the NLOS reception to some extent. To avoid this, we propose to correct the NLOS-induced error, which is presented in the following section.

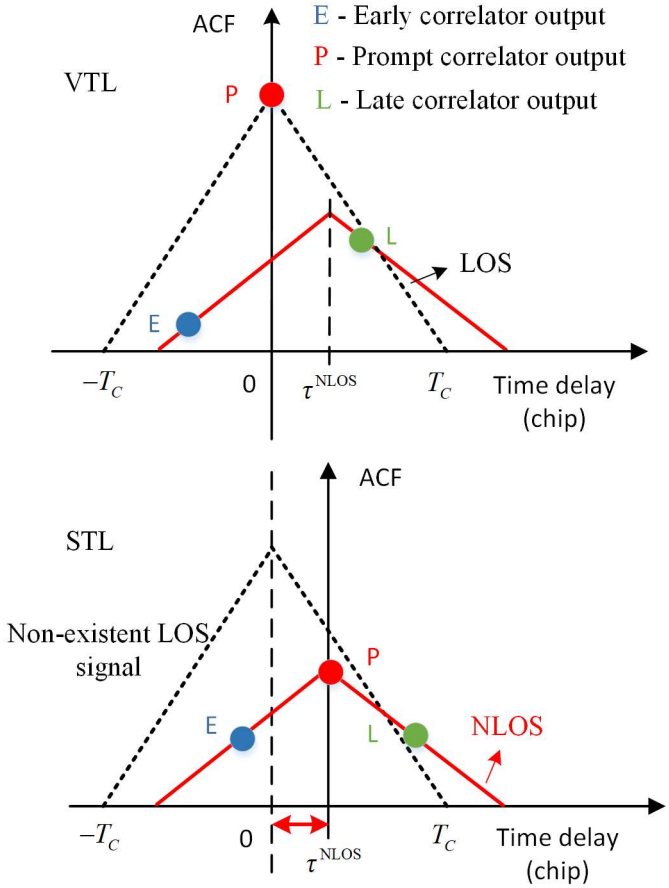

Fig. 3. Demonstration of the NLOS effects on the ACF in the VTL and STL.

This article has been accepted for publication in a future issue of this journal, but has not been fully edited. Content may change prior to final publication. Citation information: DOI 10.1109/TIM.2019.2950578, IEEE Transactions on Instrumentation and Measurement

3) Equivalent Noise Bandwidth of VTL

The objective of this paper is to design a robust NLOS detection and correction algorithm using VTL based on multi-correlator. To reduce the computational load, the concept of equivalent noise bandwidth of VTL is used to determine potential NLOS reception so as not to apply multi-correlator for all satellites. Equivalent noise bandwidth of VTL was original used for signal quality monitoring in [45]. The equivalent noise bandwidth, also simply termed as noise bandwidth, is defined as [46]

$$B_n = \int_0^{\infty} \left| \frac{H(j\omega)}{H(j\omega)_{\max}} \right|^2 \mathrm{d}\omega \tag{8}$$

where $H(j\omega)$ is the system transfer function; ω is the angular frequency.

The noise bandwidth is a useful metric for controlling the amount of noise allowed in GNSS tracking loops. Given a fixed transfer function such as the conventional 2nd-order DLL, the noise bandwidth can be determined using (8). Analogously, for the VTL with a transfer function calculated as [45]

$$H_{VTL}(s) = \left(s\mathbf{I} + \frac{\mathbf{H}_{p,k}\mathbf{G}_{p,k}}{\lambda_{CA}T_0} \right)^{-1} \frac{\mathbf{H}_{p,k}\mathbf{G}_{p,k}}{\lambda_{CA}T_0} \tag{9}$$

where $\mathbf{H}_{p,k}$ and $\mathbf{G}_{p,k}$ are the position and user clock bias part of the measurement matrix, $\mathbf{H}_k$, and the Kalman gain matrix, $\mathbf{G}_k$, respectively, the VTL noise bandwidth can be calculated using [45]

$$B_n = \frac{diag\left(\mathbf{H}_{p,k}\mathbf{G}_{p,k}\right)}{4\lambda_{CA}T_0} \tag{10}$$

where λ_{CA} denotes the width of one code chip in meters.

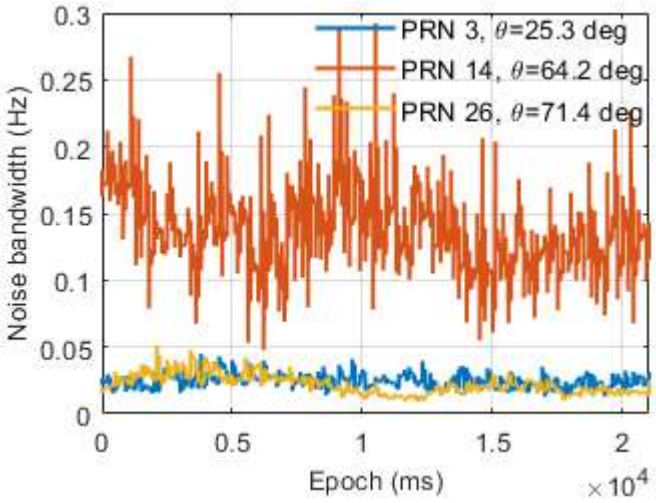

Fig. 4. Example of the noise bandwidth in the VTL for different signal types.

Fig. 4 is an example of the noise bandwidth variation in a VTL, where PRNs 3 and 14 are both LOS satellites with an elevation angle of 25.3 degrees and 64.2 degrees, respectively; PRN 26 is an NLOS satellite with an elevation angle of 71.4 degree. As can be seen, the VTL noise bandwidth for high-elevated LOS satellites is higher than that for low-elevated LOS satellites and that for NLOS satellites. The variation of the noise bandwidth gives an insight of how VTL adaptively works with respect to different signal qualities. Namely, the VTL gives a narrower bandwidth for NLOS signals to reduce its effect on positioning.

Although, a narrower noise bandwidth is also given for LOS satellites with low signal strength, the noise bandwidth in VTL can be used as an indicator of potential NLOS signal. To do this, an appropriate threshold of noise bandwidth should be pre-determined. We collected raw GPS IF data in an open-sky area to calculate the noise bandwidth for satellites with various elevation angles. Fig. 5 presents the noise bandwidth with respect to satellite elevation angle. A third-order polynomial was used to fit the relationship between the noise bandwidth and elevation angle as

$$B_n^{\text{opensky}}(\theta_{ele}) = \sum_{i=0}^{3} a_i \theta_{ele}^i \tag{11}$$

where the coefficients a_i are estimated using the least-squares method. With the estimated coefficients, a_i, we set the threshold for potential NLOS reception as 80% of the expected value calculated with (11), considering the attenuation of the reflected signal. For each satellite, if the measured noised bandwidth is lower than this threshold, then a potential NLOS reception is claimed.

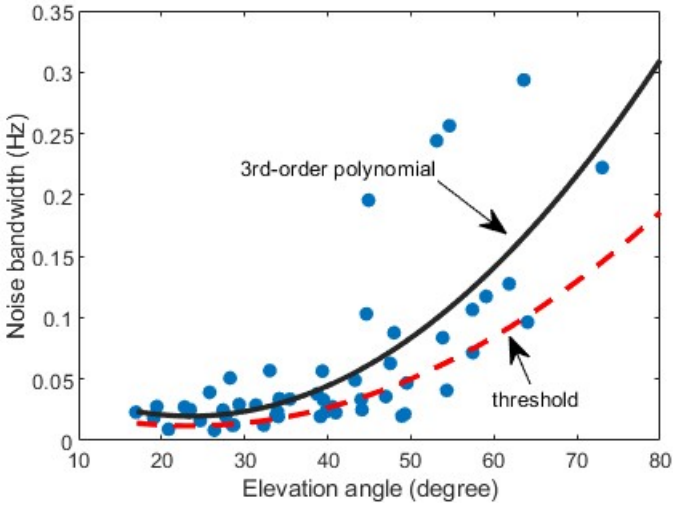

Fig. 5. Noise bandwidth for open-sky signals.

4) Algorithm Design

As shown in Fig. 4, a lower noise bandwidth cannot distinguish between NLOS satellites and low-elevated LOS satellites. An algorithm for further determination of NLOS reception is provided in this subsection. The basic idea behind this algorithm is described as below.

The VTL predicts the code frequency for each tracking channel based on the navigation solution. Given that the navigation solution is not severely affected by NLOS measurements, the NLOS signal would not be locked onto. Instead, the VTL would track the non-existent LOS signal continuously. In this way, the phase difference between the code in the incoming NLOS signal and the predicted code

This article has been accepted for publication in a future issue of this journal, but has not been fully edited. Content may change prior to final publication. Citation information: DOI 10.1109/TIM.2019.2950578, IEEE Transactions on Instrumentation and Measurement

replica would appear and manifest itself as a code tracking error, i.e., the code discriminator output. Compared to the direct LOS signal, the NLOS signal has a positive time delay. Therefore, the NLOS signal would be aligned with the code replica with a late time delay. In another word, the correlation peak has a positive time delay, which will confirm the NLOS reception. Algorithm 1 gives the detailed steps. In Step 2 of Algorithm 1, to reduce the potential NLOS effect on positioning and on the NLOS detection performance, we suggest two solutions. One is to furtherly decrease the associated noise bandwidth when there are adequate satellites. If there are limited available satellites, removing satellites will probably lead to poor satellite distribution and degraded positioning accuracy. In this case, the positioning result remains unchanged during the NLOS detection period.

Note that multi-correlator is used in Algorithm 1. In this paper, we use multiple correlators with a spacing of 0.05 chip. The benefits of the usage of multi-correlator are twofold. On the one hand, the time delay of multi-correlator peaks in vector tracking is exactly the NLOS reception time delay in principle, which provides a possible way of correcting the NLOS-induced measurement error. On the other hand, the time delay of multi-correlator peaks helps to distinguish between multipath signal and NLOS reception. For multipath signal, the code discriminator output can be either negative or positive depending on the phase difference between the reflected signal and direct signal.

Once detected, the NLOS-induced measurement error is corrected according to the detected time delay of the NLOS reception. The correction is applied using

$$\delta\rho_c^j = \left(\Delta\tau^j + \tau_{corr}\right)\cdot\frac{c}{f_{CA}} \tag{12}$$

where τ_{corr} is the NLOS correction calculated as the mean of 20 consecutive code discriminator outputs.

Algorithm 1: NLOS detection process

Input: Potential NLOS subset with M $(M>0)$ elements, noise bandwidth of the j-th satellite in the potential NLOS subset, B_n^j

Output: Deterministic NLOS subset

Steps:

1: **for** $j = 1, 2, \cdots, M$
2: Decrease B_n^j to reduce the potential NLOS effect on positioning or keep the positioning result unchanged during the NLOS detection period
3: Activate multi-correlator for the j-th satellite
4: Find the time delay of multi-correlator peaks and code discriminator outputs averaged over 20 ms, denoted as $\bar{d}_j$ and $\Delta\bar{\tau}_j$, respectively
5: **if** $\bar{d}_j > -0.05$ && $\Delta\bar{\tau}_j < 0.05$
6: Add the j-th satellite to the deterministic NLOS subset
7: **else**
8: Deactivate multi-correlator and recover the noise bandwidth for the j-th satellite
9: **end if**
10: **end for**

III. Experimental Results

This section presents experimental results to evaluate the effectiveness of the proposed method. Two field tests in urban areas in Hong Kong were conducted using real and controlled NLOS reception, respectively. One simulation test was also carried out to assess the performance of NLOS correction using NLOS receptions with controllable time delays and reflection coefficients.

A. Data Collection Equipment

Fig. 6 shows data collection equipment. The NSL Stereo front-end was used to collect the raw GPS IF data. An active antenna, Allystar AGR6303, was used due to its excellent noise performance. The raw IF data was stored on a Laptop for post-processing by a self-developed open-source VTL-based GPS software receiver [39]. Detailed configurations of the equipment are summarized in Table II.

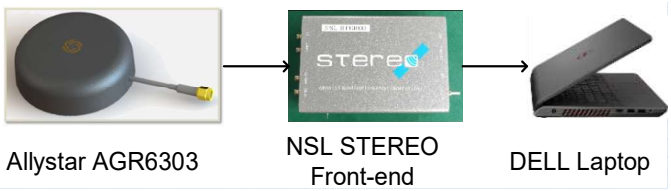

Fig. 6. Data collection equipment.

TABLE II
Parameter Settings of the Data Collection Equipment

Equipment	Parameter	Value	Unit
Antenna	Polarization	Right-hand circularly polarized (RHCP)	-
	Low noise amplifier (LNA) gain	27	dB
	Noise figure	≤ 2	dB
Front-end	GNSS signal	GPS L1 C/A	-
	Sampling rate	26	MHz
	Intermediate frequency	0	MHz
	Double-sided bandwidth	8	MHz
	Noise figure	8	dB
	Radio frequency (RF) gain	10	dB
SDR	Correlator numbers	25	-
	Correlator spacing	0.05	chip
	Coherent integration time	1	ms
	Code phase discriminator	Normalized noncoherent early minus late envelope [44]	-
	Carrier phase discriminator	Two-quadrant arctangent [44]	-

B. Test Results and Analysis

1) Test I: Real NLOS Reception

This test is intended for performance assessment of the proposed NLOS detection and correction algorithm in real applications. The test was performed in an urban area as shown in Fig. 7. The pedestrian kept static at Point 1 for about 40 seconds before walking towards east to Point 2 with an eastern velocity of around 1 m/s. After staying for about 25 seconds at Point 2, the pedestrian returned to Point 1 along the same trajectory.

This article has been accepted for publication in a future issue of this journal, but has not been fully edited. Content may change prior to final publication. Citation information: DOI 10.1109/TIM.2019.2950578, IEEE Transactions on Instrumentation and Measurement

Fig. 7. Experimental environments. (a) Top view on the Google Earth; (b) Photo looking from west to east.

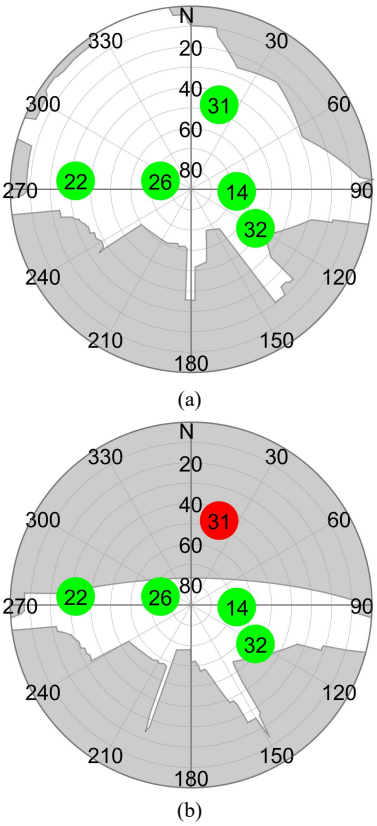

Fig. 8. Skyplots with building boundary information at (a) Points 1 and (b) 2.

The skyplots with surrounding building information, also referred to as skymask, at Points 1 and 2 are given in Fig. 8. At Point 1, five satellites are acquired and tracked successfully by the software receiver. All these five satellites are visible according to the skymask. At Point 2, however, PRN 31 is blocked by the building on the north side.

a) NLOS Detection Results

As can be seen in Fig. 7, the pedestrian moves towards east with almost no movement in the northern direction. Therefore, the velocity can be used as a reference for determining the pedestrian's state. Fig. 9 shows the horizontal velocity and noise bandwidth in the VTL. At Point 1, the noise bandwidth in all channels are at the regular level, whereas at Point 2, the noise bandwidth for PRNs 31 and 22 drops below the threshold as described in Section II. These two satellites are grouped into the potential NLOS subset.

Fig. 10 is the code discriminator output of PRN 31 in both STL and VTL. Different phenomena are observed during the period of 2750 to 4000 epochs. In the STL, the code discriminator outputs fluctuate around zeros. However, the VTL reports negative code discriminator outputs with slight oscillations during this period, which furtherly indicates the NLOS reception. To confirm this, as shown in Algorithm 1, the time delay of multi-correlator peaks should be checked, with results shown in Fig. 11. As can be seen in Fig. 11, at Point 2, there's a positive time delay of multi-correlator peaks in the VTL, which indicates that the code in the incoming signal is aligned in a late correlator. The code delay of this late correlator is yet to be found. For the STL, the time delay of multi-correlator peaks is still distributed around zeros. This phenomenon can also be seen in the ACF of the multi-correlator, as shown in Fig. 12 where the multi-correlator outputs are overlapped for 20 ms. These results confirm that PRN 31 is an NLOS satellite.

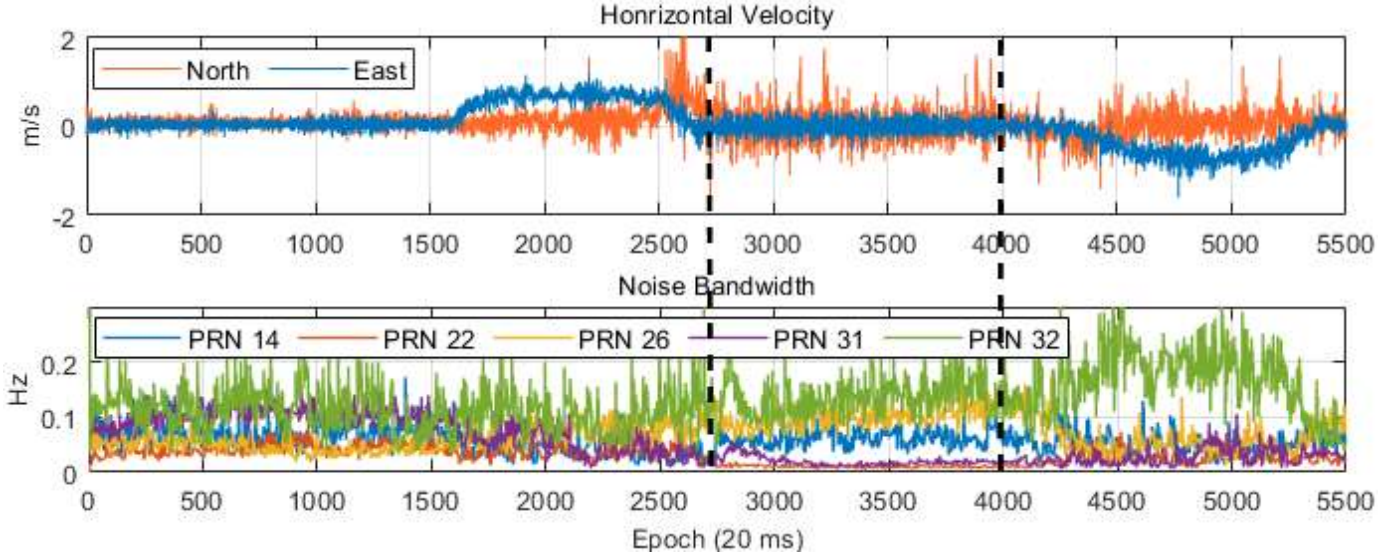

Fig. 9. User velocity and noise bandwidth in all channels.

This article has been accepted for publication in a future issue of this journal, but has not been fully edited. Content may change prior to final publication. Citation information: DOI 10.1109/TIM.2019.2950578, IEEE Transactions on Instrumentation and Measurement

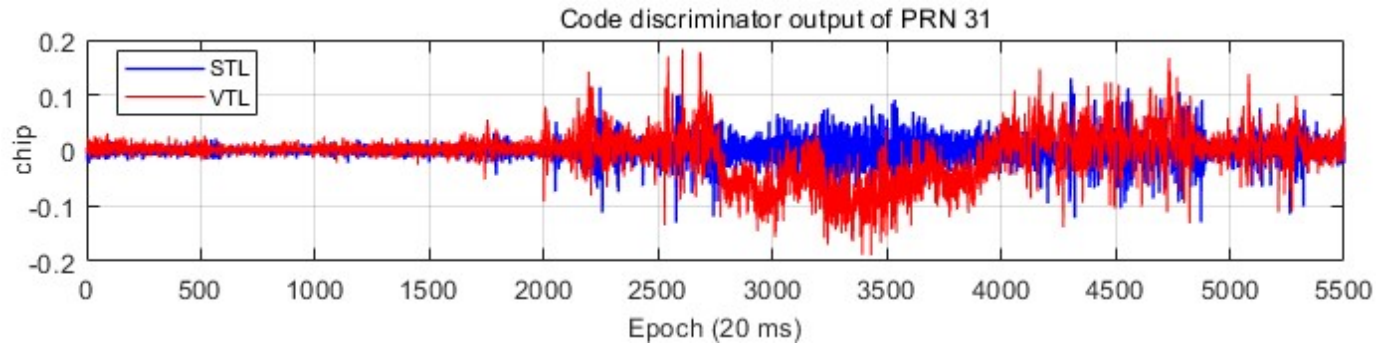

Fig. 10. Code discriminator outputs for PRN 31.

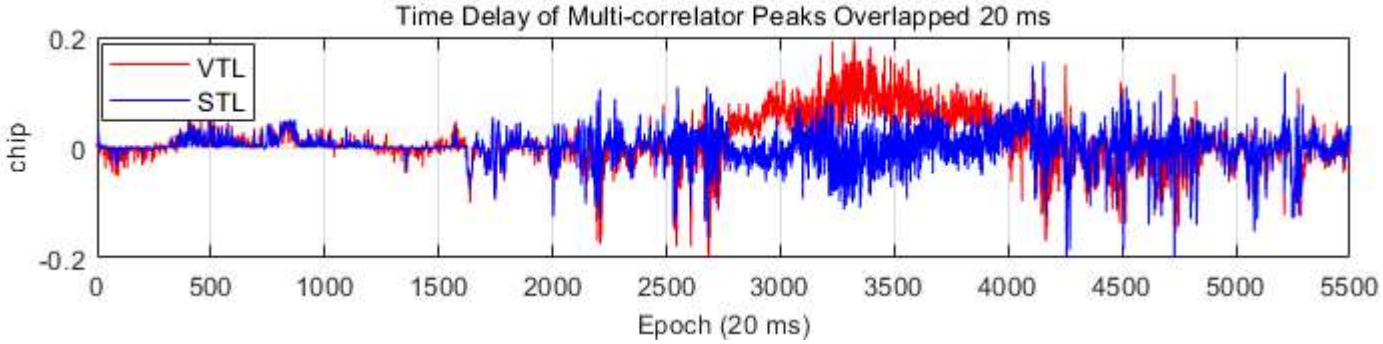

Fig. 11. Time delay of the multi-correlator peaks for PRN 31.

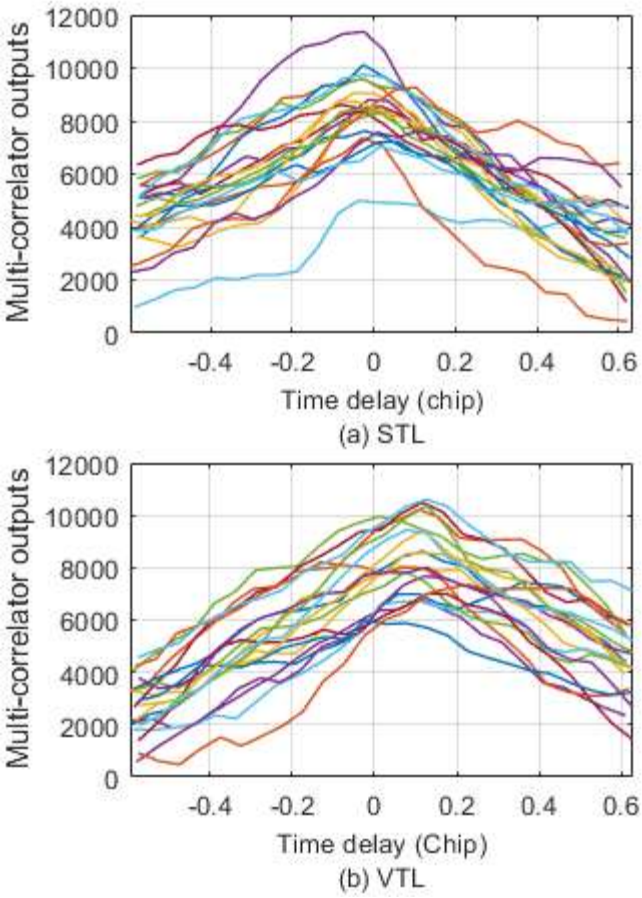

Fig. 12. Multi-correlator outputs overlapped for 20 ms of PRN 31 at 68 s for (a) STL (b) VTL.

Fig. 13 shows code discriminator outputs of PRN 22. Negative code discriminator outputs are not observed during the period of 2750 to 4000 epochs. Instead, small positive values with slight oscillations are reported. As mentioned in Section II, this is an indicator of potential multipath signal. In the VTL, a narrower noise bandwidth will be adaptively given to the multipath signal to reduce its effect on positioning.

b) NLOS Correction Results

In this test, only five satellites are available. To avoid distorting the satellite distribution, the positioning result retains unchanged during the NLOS detection period. After confirming the NLOS reception, the induced measurement error is corrected using (12). To evaluate the positioning performance, we divide the testing time into four periods, i.e., Epochs 1~1600, 1601~2750, 2751~4000, and 4001~5500, corresponding to the pedestrian's state of keeping static at Point 1, walking towards Point 2, keeping static at Point 2, and returning to Point 1, respectively.

In this test, we started correcting the NLOS-induced error from the 3000th epoch. The extracted time delay in meters of the NLOS reception is shown in Fig. 14. In [31], the NLOS pseudorange delay, $\delta\rho^{\mathrm{NLOS}}$, is modeled as

$$\delta\rho^{\mathrm{NLOS}} = \beta \sec\theta_{ele}\left(1+\cos 2\theta_{ele}\right) \tag{13}$$

where β is the distance between the receiver and building that reflects the signal; θ_{ele} is the satellite elevation angle. As shown in Fig. 15, β is around 20 meters in this test. The elevation angle of PRN 31 is 46.2 degree. Therefore, the NLOS code delay is about 26.8 meters. Notice that (1) assumes that there's only one reflected signal. In this test, the oscillation phenomenon in Figs. 10 and 14 is likely to be caused by the carrier phase change due to satellite motion. Another

This article has been accepted for publication in a future issue of this journal, but has not been fully edited. Content may change prior to final publication. Citation information: DOI 10.1109/TIM.2019.2950578, IEEE Transactions on Instrumentation and Measurement

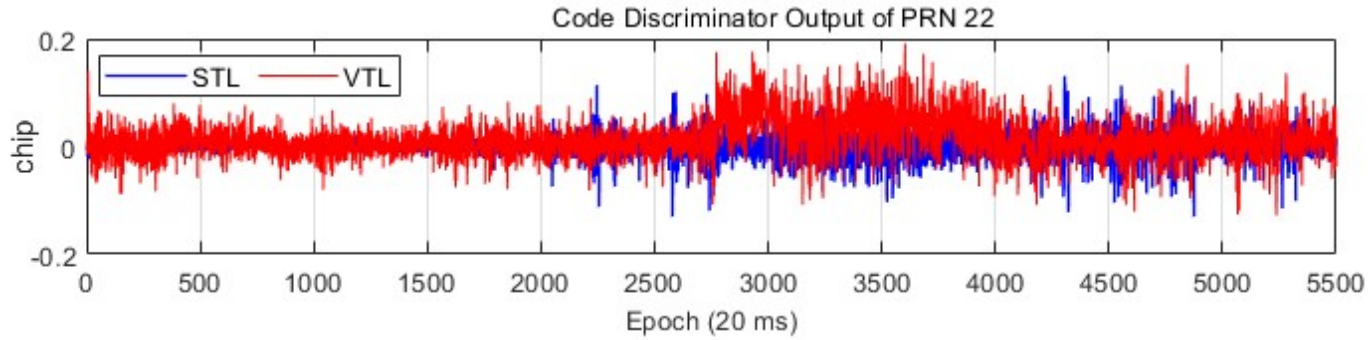

Fig. 13. Code discriminator outputs for PRN 22.

potential factor is multiple reflected NLOS signals. Like the multipath signal, the phase difference between multiple NLOS signals can also cause this oscillation.

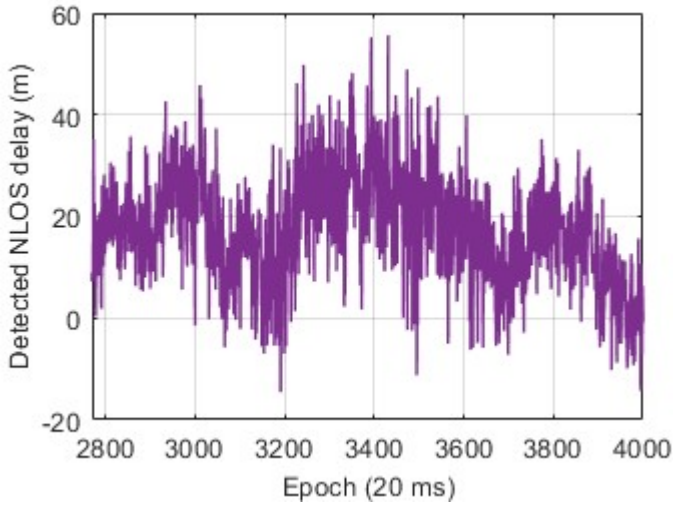

Fig. 14. Detected NLOS delay for PRN 31.

The horizontal positioning error of the STL, VTL with NLOS exclusion, and VTL with NLOS correction are shown in Fig. 16 and listed in Table III quantitatively. Overall, the VTL outperforms the STL. Specially, the VTL's superiority over STL for both the static and dynamic periods is due to the internal aiding between channels. In the third period, with the NLOS detection and correction, the horizontal positioning error decreases from 22.07 m (mean) for STL to 17.54 m (mean). A slight increase of standard deviation is also reported in the VTL in this period, which is due to the continuous NLOS correction. For the VTL with NLOS detection and exclusion, the mean positioning error increases to 23.20 m due to the distortion of horizontal dilution of precision (HDOP) (from 1.79 to 8.54) [47]. These results verify the effectiveness of the proposed algorithm.

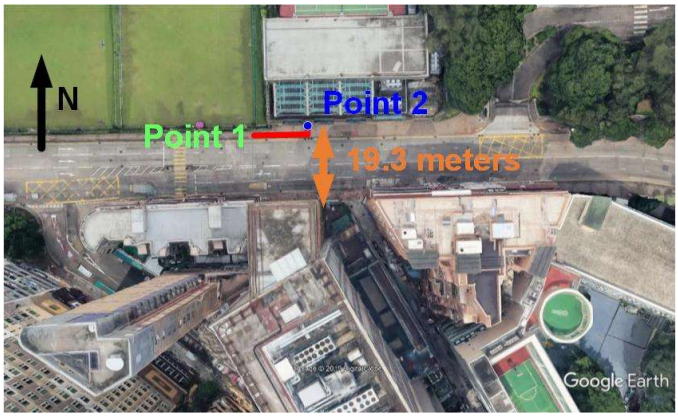

Fig. 15. Horizontal distance between the reflector and the receiver.

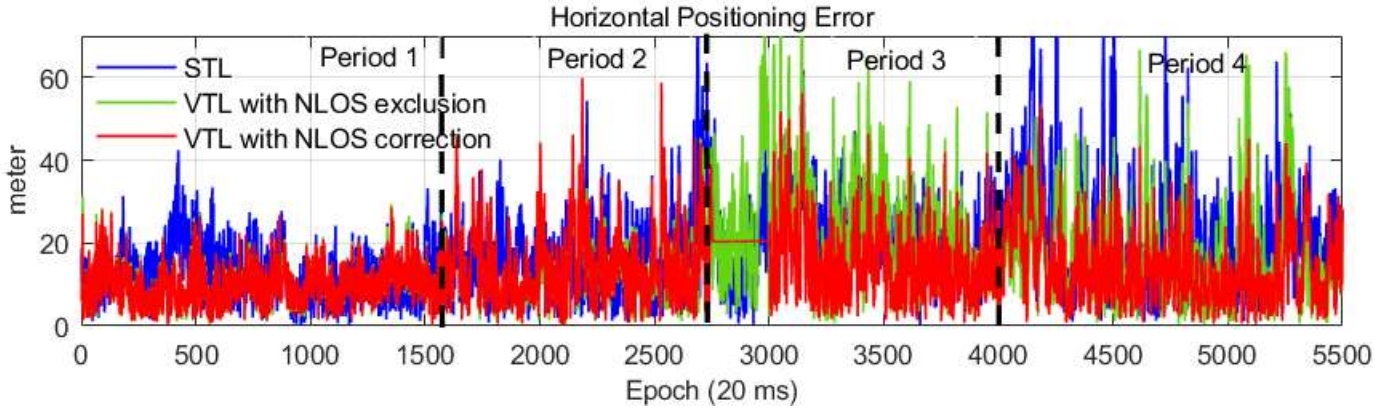

Fig. 16. Horizontal positioning error for the STL, VTL with NLOS exclusion and VTL with NLOS correction.

This article has been accepted for publication in a future issue of this journal, but has not been fully edited. Content may change prior to final publication. Citation information: DOI 10.1109/TIM.2019.2950578, IEEE Transactions on Instrumentation and Measurement

TABLE III
HORIZONTAL POSITIONING ERROR IN DIFFERENT PERIODS DURING THE TEST (METERS)

Period	STL		VTL with NLOS exclusion		VTL with NLOS correction	
	Mean	Standard deviation	Mean	Standard deviation	Mean	Standard deviation
1	12.70	6.49	10.06	4.94	9.91	4.81
2	17.24	10.23	14.26	9.15	14.42	9.23
3	22.07	8.35	23.20	13.75	17.54	10.10
4	22.83	15.03	17.54	11.64	16.00	9.79

2) Test II: Controlled NLOS Reception

In this test, the NLOS reception was generated in a controlled environment by intentionally blocking the direct signal, leading to the reception of only the reflected signal. To effectively block the direct signal during data collection, we followed the following steps:

Firstly, we selected the experimental point located at one side of the building, as shown in Fig. 17, in order to receive multipath signal at the beginning of data collection.

Secondly, data collection time was chosen with the help of 3D building model and GNSS-Radar, a web application to show the GNSS constellation at a specified time and location [48].

Thirdly, considering that the GNSS orbit retains almost unchanged at the same time on two consecutive days, we employed the ray tracing technique to confirm the reception of multipath signal for specific satellites. The elevation angle of the obstructor and the distance between obstructor and receiver antenna can also be set properly.

The whole IF data length was about 70 s. After about 40 s, we blocked the direct signal using the obstructor for about 20 s. Ray tracing result of the PRN 3 is shown in Fig. 17. Fig. 18 depicts the skymask during period of signal blockage. It is observed that the direct signal of PRN 3 is blocked, and its reflected signal is received, which can be verified by its signal strength variation, namely carrier to noise ratio (C/N_0), and the decoded navigation bit stream as shown in Figs. 19 and 20. In this test, the SDR processed the raw IF data with a skip of 5 s from the beginning of the IF file. In addition, VTL started 2 s later after the initialization by STL. As shown in Fig. 19, before the blockage of direct signal of PRN 3, the fluctuation of C/N_0 indicates the reception of multipath signal. During the blockage period, the C/N_0 decreases, which corresponds to the decrease of correlation value in Fig. 20.

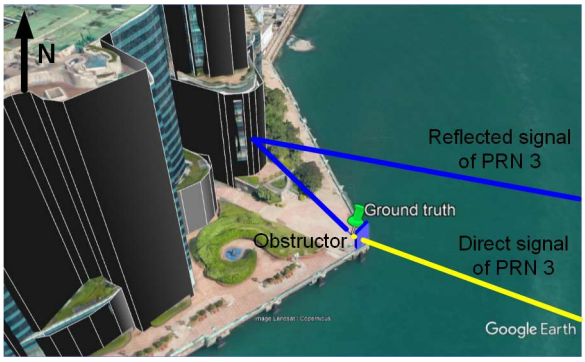

Fig. 17. Ray tracing result of PRN 3.

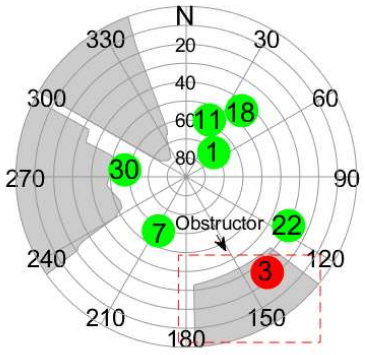

Fig. 18. Skymask during data collection.

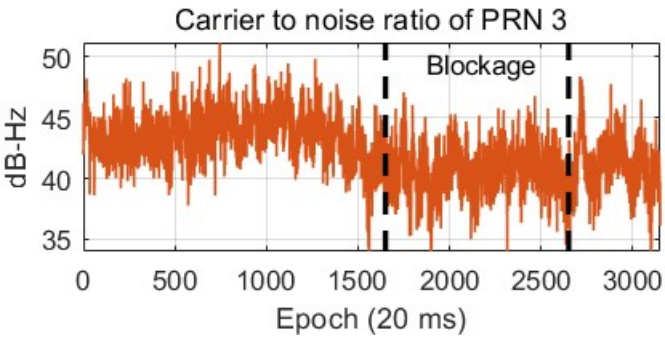

Fig. 19. Carrier to noise ratio of PRN 3 in VTL.

This article has been accepted for publication in a future issue of this journal, but has not been fully edited. Content may change prior to final publication. Citation information: DOI 10.1109/TIM.2019.2950578, IEEE Transactions on Instrumentation and Measurement

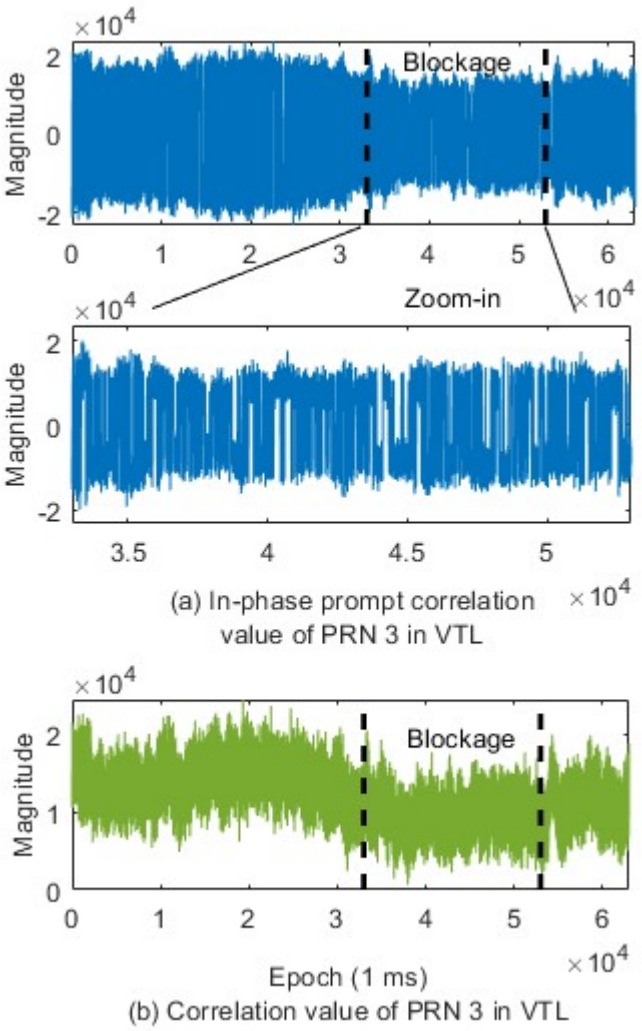

Fig. 20. Tracking results of PRN 3 in VTL. (a) In-phase prompt correlation value; (b) Correlation value of PRN 3.

The noise bandwidth of PRN 3 during the test is shown in Fig. 21. The decrease of the noise bandwidth during the period of artificial blockage indicates the degraded signal quality, which is considered potential NLOS reception by the proposed algorithm.

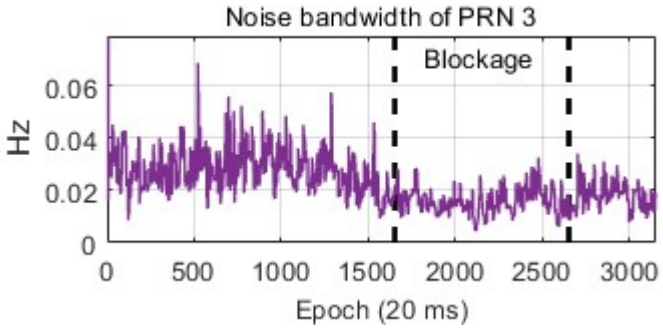

Fig. 21. Noise bandwidth of PRN 3 in VTL.

Figs. 22 and 23 show the code discriminator output of PRN 3 and time delay of multi-correlator peaks based on STL and VTL, respectively. During the period of direct signal blockage, VTL reports negative code discriminator outputs of PRN 3 during most time of the period of signal blockage, whereas the STL tightly locks onto the signal, leading to the fluctuation of code tracking error around zeros. In addition, during the direct signal blockage of PRN 3, VTL has a positive time delay of multi-correlator peaks, which are distributed around zeros in STL. This result is consistent with that in Test I.

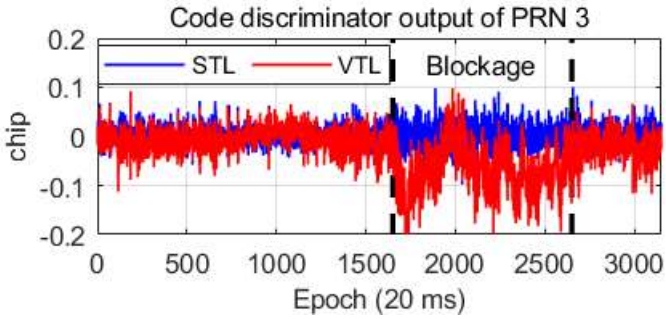

Fig. 22. Code discriminator output of PRN 3.

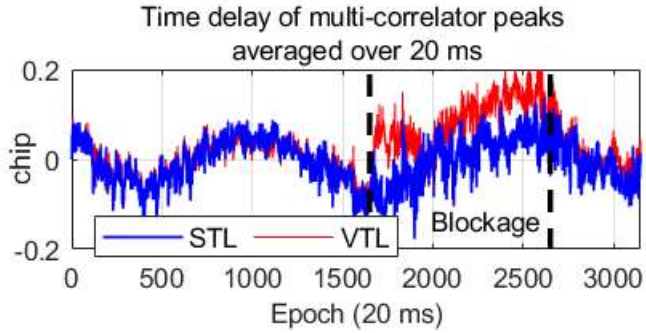

Fig. 23. Time delay of multi-correlator peaks averaged over 20 ms of PRN 3.

Fig. 24 shows the detected pseudorange error of PRN 3. As can been seen, the detected code delay of NLOS reception varies with time. Unlike using (13) to assess the performance of NLOS-induced pseudorange measurement error detection, in this test, we adopted the metric of code pseudorange double difference (DD) observable shown in Fig. 24, which can be considered as the pseudorange error mainly caused by NLOS or multipath effects [49]. The definition and calculation of DD can be found in [49]. In this paper, the reference station was chosen as the HKSC station of SatRef, which is established by the Hong Kong land department for providing differential corrections. It is observed that, the DD observable during the signal blockage period varies with time and its mean value is 31.7 meters. Note that, during epochs 1 to 20 s, the DD observable also shows positive values, which is due to multipath effects. The detected NLOS-induced pseudorange measurement error of PRN 3 has a mean value of 19.5 meters.

This article has been accepted for publication in a future issue of this journal, but has not been fully edited. Content may change prior to final publication. Citation information: DOI 10.1109/TIM.2019.2950578, IEEE Transactions on Instrumentation and Measurement

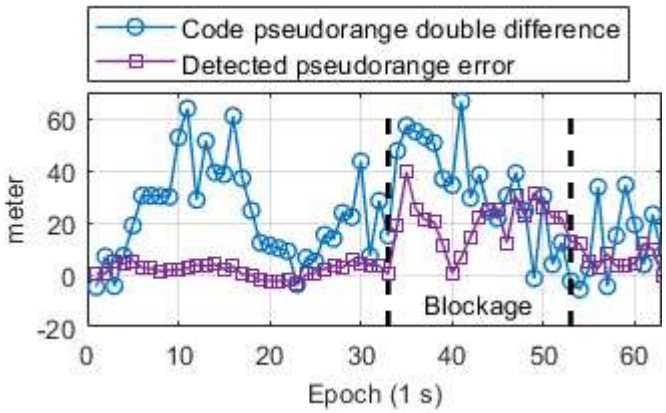

Fig. 24. Detected pseudorange error of PRN 3 with comparison to code pseudorange double difference.

The horizontal positioning error based on STL, VTL with NLOS exclusion, and VTL with NLOS correction is shown in Fig. 25. Compared to STL, VTL with both NLOS exclusion and correction shows lower positioning error than STL, which has explained in Test I. Note that, the positioning error has no obvious improvement with NLOS correction over that with NLOS exclusion. The reason is that the NLOS-induced positioning error is less dominant than that caused by multipath. In addition, in this test, the HDOP values before and after blockage of direct signal of PRN 3 are 1.85 and 1.87, respectively. As such, exclusion of PRN 3 has little effect on the positioning accuracy.

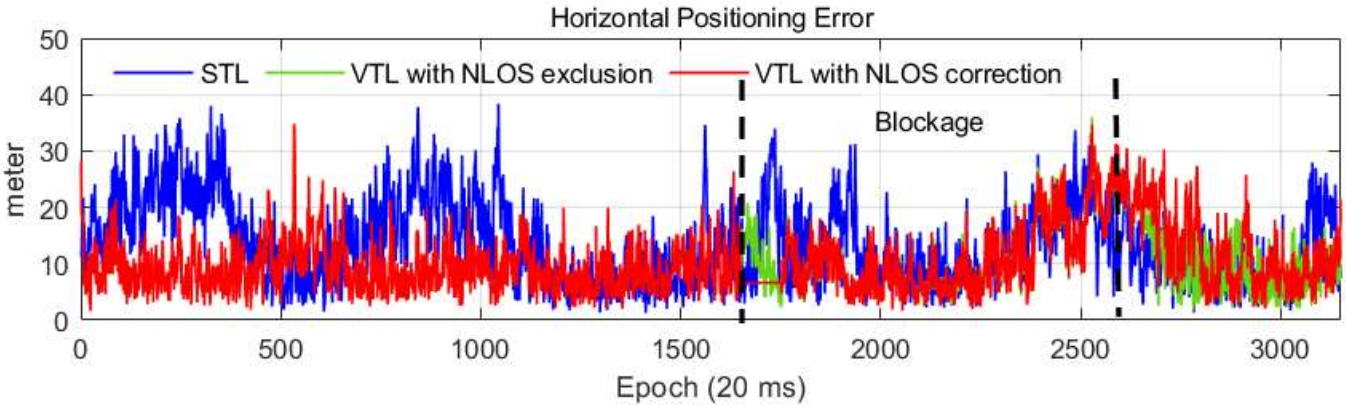

Fig. 25. Horizontal positioning error for the STL, VTL with NLOS exclusion and VTL with NLOS correction.

C. Performance Assessment of NLOS Correction

The effectiveness of the proposed algorithm has been validated in the two field tests. In this part, the accuracy of NLOS correction is assessed using simulated NLOS receptions with controllable time delays and reflection coefficients to reveal the performance bounds of the proposed method.

The NLOS reception is simulated using an algorithm called direct signal cancelation [28]. To simulate NLOS reception, GPS raw IF data is first collected and processed using a software GPS receiver. A relatively strong signal replica is then generated according to the tracking parameters such as phase and frequency of the code and carrier, decoded navigation data, and the estimated signal amplitude. By subtracting the signal replica from the raw data, and then adding a code-delayed version of the signal replica to the original data, a dataset that contains the NLOS reception can be generated. One advantage of this algorithm is that the code delay and amplitude of the NLOS reception can be exactly controlled to better evaluate the proposed NLOS correction method. In this paper, we use the root mean square error (RMSE) as the metric for assessing the NLOS correction performance.

In VTL, the code frequency is predicted based on the navigation solution. Therefore, the accuracy of the navigation solution is directly related to the NLOS correction performance. Fig. 26 shows the simulation result of the NLOS correction performance regarding horizontal positioning errors. The NLOS time delay is 0.15 chip with a reflection coefficient of 0.6. As observed in Fig. 26, the NLOS correction performance highly relies on the positioning accuracy.

Fig. 27 shows the RMSE with regards to the reflection coefficient for different NLOS time delays. In these simulations, the RMSE of the horizontal position during the NLOS detection period is around 10 meters. Several conclusions can be drawn according to the results: i) The RMSE of NLOS correction decreases with the increase of reflection coefficient. The accuracy improvement is greater at low reflection coefficients than that at high reflection coefficients; ii) For the same reflection coefficient, the NLOS correction performance increases with larger time delays, which is more obvious for the reflection coefficients in the range of 0.2 to 0.4; iii) It's difficult to correct the NLOS error for short time delays, e.g., less than 0.05 chip.

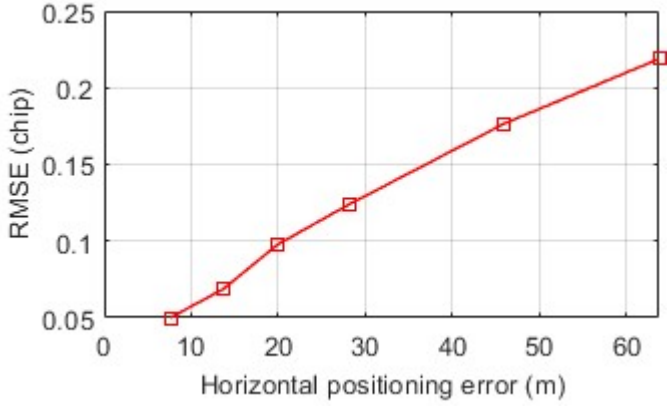

Fig. 26. The NLOS correction performance regrading horizontal positioning errors.

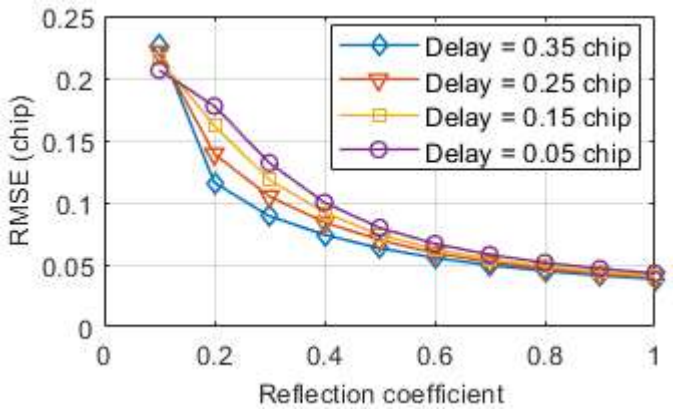

Fig. 27. The NLOS correction performance for different time delays regarding reflection coefficients.

IV. Conclusion

In this paper, we analyzed the NLOS effects on both scalar and vector tracking loops mathematically, based on which an NLOS detection and correction algorithm using the VTL was proposed. We used the metric of equivalent noise bandwidth of VTL to find potential NLOS reception, and then confirmed it using the time delay of multi-correlator peaks and code discriminator output. The NLOS-induced measurement error was furtherly corrected before being fed forward into the Kalman filter. Two kinds of NLOS reception, namely the real-world NLOS reception and the NLOS reception generated by intentionally blocking direct signal, were used to test the proposed algorithm. We also simulated NLOS receptions with controllable time delays and reflection coefficients to demonstrate the NLOS correction performance in different scenarios. This method requires no additional aiding, which is more feasible for instrumentation where GNSS receivers are embedded. A promising extension of this work is to correct the multipath-induced measurement error and spoofing mitigation using VTL-based GNSS SDR [28, 50].

Appendix I

Proof of the Code Discriminator Output

For a binary phase shift key (BPSK) signal such as the GPS L1 C/A signal, the autocorrelation function is defined as [4]

$$R(\tau)=\begin{cases}1-\dfrac{|\tau|}{T_c}, & |\tau|\le T_c\\ 0\end{cases}$$
$$=\begin{cases}1+\dfrac{\tau}{T_c}, & -T_c<\tau\le 0\\ 1-\dfrac{\tau}{T_c}, & 0<\tau\le T_c\\ 0\end{cases} \quad \text{(A1)}$$

where $\tau=\tau_{\text{replica}}-\tau_{\text{incoming}}$ is the difference between the local code replica phase, τ_{replica}, and the code phase in the incoming signal, τ_{incoming}; T_c is the code duration. For simplicity, we consider the signal amplitude as 1, assume perfect carrier tracking and ignore the nose. The early and late correlator outputs can then be simplified as

$$E(n)=R\left(\tau+\frac{d}{2}\right)$$
$$=\begin{cases}1+\dfrac{\tau+\frac{d}{2}}{T_c}, & -T_c-\dfrac{d}{2}<\tau\le-\dfrac{d}{2}\\ 1-\dfrac{\tau+\frac{d}{2}}{T_c}, & -\dfrac{d}{2}<\tau\le T_c-\dfrac{d}{2}\\ 0, & \text{otherwise}\end{cases} \quad \text{(A2)}$$

$$L(n)=R\left(\tau-\frac{d}{2}\right)$$
$$=\begin{cases}1+\dfrac{\tau-\frac{d}{2}}{T_c}, & -T_c+\dfrac{d}{2}<\tau\le\dfrac{d}{2}\\ 1-\dfrac{\tau-\frac{d}{2}}{T_c}, & \dfrac{d}{2}<\tau\le T_c+\dfrac{d}{2}\\ 0, & \text{otherwise}\end{cases} \quad \text{(A3)}$$

where $d=T_c$ is the spacing between the Early and Late correlators. For the code discriminator, normalized noncoherent early minus late envelope [44], we have

$$\begin{aligned}\Delta\tau(n) &= \frac{1}{2}\frac{E(n)-L(n)}{E(n)+L(n)} \\ &= \frac{1}{2}\frac{-\frac{2\tau}{T_c}}{2-\frac{d}{T_c}}, \quad -\frac{T_c}{2}<\tau\le\frac{T_c}{2} \\ &= -\frac{\tau}{T_c}, \quad -\frac{T_c}{2}<\tau\le\frac{T_c}{2}\end{aligned} \tag{A4}$$

APPENDIX II
Modelling of EKF-based VTL

In this paper, an error state based EKF is used as the navigation solver. The error state is expressed as

$$\delta\mathbf{x} = \left[\delta\mathbf{p}, \delta\mathbf{v}, \delta b, \delta d\right]^T \tag{A5}$$

where $\delta\mathbf{p} = \left[\delta p_x, \delta p_y, \delta p_z\right]$ and $\delta\mathbf{v} = \left[\delta v_x, \delta v_y, \delta v_z\right]$ are the 3D user position and velocity errors in the Earth-centered Earth-fixed (ECEF) coordinate system, respectively, δb and δd are the receiver clock bias and drift error in meters and meters per second, respectively. The superscript T denotes the transpose of a matrix. The system propagation at epoch k is

$$\delta\mathbf{x}_{k|k-1} = \mathbf{\Phi}\delta\mathbf{x}_{k-1} + \mathbf{w}_{k-1} \tag{A6}$$

where $\mathbf{w}$ is the system noise vector, $\mathbf{\Phi}$ is the constant transition matrix given by

$$\mathbf{\Phi} = \begin{bmatrix}\mathbf{I}_{3\times3} & T_0\mathbf{I}_{3\times3} & \mathbf{0}_{3\times2} \\ \mathbf{0}_{3\times3} & \mathbf{I}_{3\times3} & \mathbf{0}_{3\times2} \\ \mathbf{0}_{2\times3} & \mathbf{0}_{2\times3} & \mathbf{K}\end{bmatrix}_{8\times8} \tag{A7}$$

$$\mathbf{K} = \begin{bmatrix}1 & T_0 \\ 0 & 1\end{bmatrix} \tag{A8}$$

where T_0 is the EKF update interval. The covariance matrix of $\mathbf{w}$ is set according to the rule of thumb values based on the user dynamics or calculated using [28]

$$\mathbf{Q} = \begin{bmatrix}\mathbf{Q}_{dyn} & \mathbf{0}_{6\times2} \\ \mathbf{0}_{2\times6} & \mathbf{Q}_{clk}\end{bmatrix} \tag{A9}$$

$$\mathbf{Q}_{dyn} = \begin{bmatrix}T_0^3/3\cdot\mathbf{I}_{3\times3} & T_0^2/2\cdot\mathbf{I}_{3\times3} \\ T_0^2/2\cdot\mathbf{I}_{3\times3} & T_0\cdot\mathbf{I}_{3\times3}\end{bmatrix}\cdot S_v \tag{A10}$$

$$\mathbf{Q}_{clk} = \begin{bmatrix}S_f\cdot T_0 + S_g T_0^3/3 & S_g T_0^2/2 \\ S_g T_0^2/2 & S_g\cdot T_0\end{bmatrix} \tag{A11}$$

where S_v is the receiver velocity noise power spectral density (PSD); S_f and S_g are the PSD of receiver clock phase and frequency, respectively. The value of S_v should be set according to the level of user dynamics. Settings of S_f and S_g are calculated using the following formulas

$$S_f = c^2\cdot h_0/2 \tag{A12}$$

$$S_g = c^2\cdot 2\pi^2\cdot h_{-2} \tag{A13}$$

where h_0 are h_{-2} the coefficients of white frequency modulation noise and random walk frequency modulation noise of the oscillator used, respectively. The priori estimation covariance matrix, $\mathbf{P}_{k|k-1}$, is

$$\mathbf{P}_{k|k-1} = \mathbf{\Phi}\mathbf{P}_{k-1}\mathbf{\Phi}^T + \mathbf{Q}_{k-1} \tag{A14}$$

The measurements of the EKF comprise the pseudorange error, $\delta\rho_k^m$, and the pseudorange rate error, $\delta\dot{\rho}_k^m$, which are related to the user's state as

$$\delta\rho_k^m = -l_{x,k}^m\cdot\delta p_{x,k} - l_{y,k}^m\cdot\delta p_{y,k} - l_{z,k}^m\cdot\delta p_{z,k} + \delta b_k \tag{A15}$$

$$\delta\dot{\rho}_k^m = -l_{x,k}^m\cdot\delta v_{x,k} - l_{y,k}^m\cdot\delta v_{y,k} - l_{z,k}^m\cdot\delta v_{z,k} + \delta d_k \tag{A16}$$

where $-\mathbf{l}_k^m = \left[-l_{x,k}^m, -l_{y,k}^m, -l_{z,k}^m\right]$ is the unit LOS vector pointing from the receiver to the m-th satellite, which is calculated using the user position, $\mathbf{p}_k$, and the m-th satellite position, $\mathbf{p}_k^m$, as

$$-\mathbf{l}_k^m = -\left(\mathbf{p}_k^m - \mathbf{p}_k\right)/\left\|\mathbf{p}_k^m - \mathbf{p}_k\right\| \tag{A17}$$

$$\mathbf{p}_k = \mathbf{p}_{k-1} + \delta\mathbf{p}_k \tag{A18}$$

Based on (A15) and (A16), the measurement vector, $\delta\mathbf{z}_k$, is derived as

$$\delta\mathbf{z}_k = \mathbf{H}_k\cdot\delta\mathbf{x}_{k-1} + \mathbf{V}_k \tag{A19}$$

where

$$\mathbf{H}_k = \begin{bmatrix}-l_{x,k}^1 & -l_{y,k}^1 & -l_{z,k}^1 & 0 & 0 & 0 & 1 & 0 \\ -l_{x,k}^2 & -l_{y,k}^2 & -l_{z,k}^2 & 0 & 0 & 0 & 1 & 0 \\ \vdots & \vdots & \vdots & \vdots & \vdots & \vdots & \vdots & \vdots \\ -l_{x,k}^m & -l_{y,k}^m & -l_{z,k}^m & 0 & 0 & 0 & 1 & 0 \\ 0 & 0 & 0 & -l_{x,k}^1 & -l_{y,k}^1 & -l_{z,k}^1 & 0 & 1 \\ 0 & 0 & 0 & -l_{x,k}^2 & -l_{y,k}^2 & -l_{z,k}^2 & 0 & 1 \\ \vdots & \vdots & \vdots & \vdots & \vdots & \vdots & \vdots & \vdots \\ 0 & 0 & 0 & -l_{x,k}^m & -l_{y,k}^m & -l_{z,k}^m & 0 & 1\end{bmatrix}_{2m\times8} \tag{A20}$$

, $\mathbf{V}_k$ is the measurement noise vector with its covariance matrix given by

$$\mathbf{R}_k = \mathrm{diag}\left(\sigma\left(\boldsymbol{\gamma}_k\right)\right) \tag{A21}$$

where $\sigma(x)$ denotes the variance of x, $\boldsymbol{\gamma}_k = \delta\mathbf{z}_k - \mathbf{H}_k\delta\mathbf{x}_{k|k-1}$ is the measurement innovation, and $\mathrm{diag}(\cdot)$ denotes a diagonal matrix.

In the VTL, $\delta\rho_k^m$ and $\delta\dot{\rho}_k^m$ are extracted from the code and carrier tracking loops, respectively, as

$$\delta\rho_k^m = \delta\tau_k^m\cdot c/f_{CA} \tag{A22}$$

$$\delta\dot{\rho}_k^m = f_{d,k}^m\cdot c/f_{L1} - \left(\mathbf{v}_k - \mathbf{v}_k^m\right)\cdot\mathbf{l}_k^m - \delta d_k \tag{A23}$$

where $\delta\tau_k^m$ is the code discriminator output in chips, f_{CA} is the code chipping rate (1.023 MHz for GPS L1 C/A), c is the speed of light, $f_{d,k}^m$ is the measured Doppler shift frequency in hertz, f_{L1} is the carrier frequency (1575.42 MHz for GPS L1), $\mathbf{v}_k$ and $\mathbf{v}_k^m$ are the velocity vectors of the receiver and the m-th satellite, respectively.

The priori error state estimation is therefore updated given the measurement innovation, $\boldsymbol{\gamma}_k$, and the Kalman gain, $\mathbf{G}_k$, using

$$\delta\mathbf{x}_k = \delta\mathbf{x}_{k|k-1} + \mathbf{G}_k\boldsymbol{\gamma}_k \tag{A24}$$

where

$$\mathbf{G}_k = \mathbf{P}_{k|k-1}\mathbf{H}_k^T\left(\mathbf{R}_k + \mathbf{H}_k\mathbf{P}_{k|k-1}\mathbf{H}_k^T\right)^{-1} \quad \text{(A25)}$$

The posterior estimation covariance matrix is then updated using

$$\mathbf{P}_k = \left(\mathbf{I} - \mathbf{G}_k\mathbf{H}_k\right)\mathbf{P}_{k|k-1} \quad \text{(A26)}$$

With the updated error state, $\delta\mathbf{x}_k$, the total state is finally obtained as

$$\mathbf{x}_k = \mathbf{\Phi}\cdot\mathbf{x}_{k-1} + \delta\mathbf{x}_k \quad \text{(A27)}$$

REFERENCES

[1] A. Carta, N. Locci, C. Muscas, and S. Sulis, "A flexible GPS-based system for synchronized phasor measurement in electric distribution networks," *IEEE Transactions on Instrumentation and Measurement,* vol. 57, no. 11, pp. 2450-2456, 2008.

[2] D. N. Aloi, M. Alsliety, and D. M. Akos, "A methodology for the evaluation of a GPS receiver performance in telematics applications," *IEEE Transactions on Instrumentation and Measurement,* vol. 56, no. 1, pp. 11-24, 2007.

[3] C. Boucher and J. C. Noyer, "A hybrid particle approach for GNSS applications with partial GPS outages," *IEEE Transactions on Instrumentation and Measurement,* vol. 59, no. 3, pp. 498-505, 2010.

[4] W. Nam and S.-H. Kong, "Least-squares-based iterative multipath super-resolution technique," *IEEE Transactions on Signal Processing,* vol. 61, no. 3, pp. 519-529, 2013.

[5] A. Rabaoui, N. Viandier, E. Duflos, J. Marais, and P. Vanheeghe, "Dirichlet process mixtures for density estimation in dynamic nonlinear modeling: Application to GPS positioning in urban canyons," *IEEE Transactions on Signal Processing,* vol. 60, no. 4, pp. 1638-1655, 2012.

[6] X. Peng and M. G. Petovello, "Measuring GNSS multipath distributions in urban canyon environments," *IEEE Transactions on Instrumentation and Measurement,* vol. 64, no. 2, pp. 366-377, 2015.

[7] D. H. Won *et al.*, "Selective integration of GNSS, vision sensor, and INS using weighted DOP under GNSS-challenged environments," *IEEE Transactions on Instrumentation and Measurement,* vol. 63, no. 9, pp. 2288-2298, 2014.

[8] Q. Jia, R. Wu, W. Wang, D. Lu, L. Wang, and J. Li, "Multipath interference mitigation in GNSS via wrelax," *GPS Solutions,* vol. 21, no. 2, pp. 487-498, 2016.

[9] G.-Y. Chen, M. Gan, C. L. P. Chen, and L. Chen, "A two-stage estimation algorithm based on variable projection method for GPS positioning," *IEEE Transactions on Instrumentation and Measurement,* vol. 67, no. 11, pp. 2518-2525, 2018.

[10] P. D. Groves, Z. Jiang, M. Rudi, and P. Strode, "A portfolio approach to NLOS and multipath mitigation in dense urban areas," in *Proceedings of the 26th International Technical Meeting of the Satellite Division of The Institute of Navigation (ION GNSS+ 2013)*, Nashville, TN, 2013, pp. 3231-3247.

[11] M. S. Braasch, "Multipath effects," in *Global positioning system theory and applications*, vol. I, B. Parkinson, S. J. J, P. Axelrad, and P. Enge, Eds. (Progress inastronautics and aeronautics, Washington, DC: American Institute of Aeronautics and Astronautics, Inc., 1996, pp. 547-566.

[12] P. D. Groves and Z. Jiang, "Height aiding, C/N0 weighting and consistency checking for GNSS NLOS and multipath mitigation in urban areas," *Journal of Navigation,* vol. 66, no. 05, pp. 653-669, 2013.

[13] Z. Jiang and P. D. Groves, "GNSS NLOS and multipath error mitigation using advanced multi-constellation consistency checking with height aiding," in *Proceedings of ION ITM 2012*, Nashville TN, 2012, pp. 79-88.

[14] L.-T. Hsu, H. Tokura, N. Kubo, Y. Gu, and S. Kamijo, "Multiple faulty GNSS measurement exclusion based on consistency check in urban canyons," *IEEE Sensors Journal,* vol. 17, no. 6, pp. 1909-1917, 2017.

[15] M. Spangenberg, V. Calmettes, O. Julien, J.-Y. Tourneret, and G. Duchateau, " Detection of variance changes and mean value jumps in measurement noise for multipath mitigation in urban navigation," *NAVIGATION: Journal of The Institute of Navigation,* vol. 57, no. 1, pp. 35-52, 2010.

[16] A. Brown and N. Gerein, "Test results from a digital p(y) code beamsteering receiver for multipath minimization," in *Proceedings of ION 57th Annual Meeting*, Albuquerque, NM, 2001.

[17] Z. Jiang and P. D. Groves, "NLOS GPS signal detection using a dual-polarisation antenna," *GPS Solutions,* vol. 18, no. 1, pp. 15-26, 2014.

[18] J. S. Sanchez, A. Gerhmann, P. Thevenon, P. Brocard, A. B. Afia, and O. Julien, "Use of a fisheye camera for GNSS NLOS exclusion and characterization in urban environments," in *Proceedings of ION ITM 2016*, Monterey, United States, 2016.

[19] J. i. Meguro, T. Murata, J. i. Takiguchi, Y. Amano, and T. Hashizume, "GPS multipath mitigation for urban area using omnidirectional infrared camera," *IEEE Transactions on Intelligent Transportation Systems,* vol. 10, no. 1, pp. 22-30, 2009.

[20] P. D. Groves, Z. Jiang, L. Wang, and M. K. Ziebart, "Intelligent urban positioning using multi-constellation GNSS with 3D mapping and NLOS signal detection," in *Proceedings of ION ITM 2012*, Nashville, TN, 2012, pp. 458-472.

[21] R. Yozevitch, B. B. Moshe, and A. Weissman, "A robust GNSS LOS/NLOS signal classifier," *NAVIGATION: Journal of The Institute of Navigation,* vol. 63, no. 4, pp. 429-442, 2016.

[22] T. Suzuki, Y. Nakano, and Y. Amano, "NLOS multipath detection by using machine learning in urban environments," in *Proceedings of ION GNSS+ 2017*, Portland, Oregon, 2017, pp. 3958-3967.

[23] R. Sun, L.-T. Hsu, D. Xue, G. Zhang, and W. Y. Ochieng, "GPS signal reception classification using adaptive neuro-fuzzy inference system," *Journal of Navigation,* pp. 1-17, 2018.

[24] N. I. Ziedan, "Urban positioning accuracy enhancement utilizing 3D buildings model and accelerated ray tracing algorithm," in *Proceedings of the 30th International Technical Meeting of The Satellite Division of the Institute of Navigation (ION GNSS+ 2017)*, 2017.

[25] L.-T. Hsu, Y. Gu, and S. Kamijo, "NLOS correction/exclusion for gnss measurement using raim and city building models," *Sensors,* vol. 15, no. 7, pp. 17329-17349, 2015.

[26] L. Wang, P. D. Groves, and M. K. Ziebart, "Smartphone shadow matching for better cross-street GNSS positioning in urban environments," *Journal of Navigation,* vol. 68, no. 03, pp. 411-433, 2015.

[27] S. Peyraud *et al.*, "About non-line-of-sight satellite detection and exclusion in a 3D map-aided localization algorithm," *Sensors (Basel),* vol. 13, no. 1, pp. 829-47, Jan 11 2013.

[28] L.-T. Hsu, S. S. Jan, P. D. Groves, and N. Kubo, "Multipath mitigation and NLOS detection using vector tracking in urban environments," *GPS Solutions,* vol. 19, no. 2, pp. 249-262, 2015.

[29] H. F. Ng, G. Zhang, and L. T. Hsu, "Range-based 3D mapping aided GNSS with NLOS correction based on skyplot with building boundaries," in *Proceedings of the ION 2019 Pacific PNT Meeting*, Honolulu, Hawaii, 2019.

[30] W. Wen, G. Zhang, and L.-T. Hsu, "Correcting GNSS NLOS by 3D LiDAR and building height," in *Proceedings of ION GNSS+ 2018*, Miami, Florida, 2018.

[31] L.-T. Hsu, "Analysis and modeling GPS NLOS effect in highly urbanized area," *GPS Solutions,* vol. 22, no. 1, 2018.

[32] P. D. Groves, "Shadow matching: A new GNSS positioning technique for urban canyons,", *Journal of Navigation,* vol. 64, no. 3, pp. 417-430, 2011.

[33] B. Xu and L.-T. Hsu, "NLOS detection and compensation using a vector tracking-based GPS software receiver," in *Proceedings of the ION 2019 Pacific PNT Meeting*, Honolulu, Hawaii, 2019, pp. 702-712.

[34] M. Lashley, D. M. Bevly, and J. Y. Hung, "Performance analysis of vector tracking algorithms for weak GPS signals in high dynamics," *IEEE Journal of Selected Topics in Signal Processing,* vol. 3, no. 4, pp. 661-673, 2009.

[35] T. Pany and B. Eissfeller, "Use of a vector delay lock loop receiver for GNSS signal power analysis in bad signal conditions," in *Proceedings of 2006 IEEE/ION Position, Location, And Navigation Symposium*, Coronado, CA, USA, 2006, vol. 85, no. 85, pp. 893-903: IEEE.

[36] T. Lin, M. Abdizadeh, A. Broumandan, D. Wang, K. O'Keefe, and G. Lachapelle "Interference suppression for high precision navigation using vector-based GNSS software receivers," in *Proceedings of the 24th International Technical Meeting of the Satellite Division of The Institute of Navigation (ION GNSS 2011)*, Portland, OR, 2011, pp. 372-383

[37] Q. Li, Z. Han, W. Wang, X. Wang, and D. Xu, "Anti-jamming scheme for GPS receiver with vector tracking loop and blind beamformer," *Electronics Letters,* vol. 50, no. 19, pp. 1386-1388, 2014.

[38] X. Tang, G. Falco, E. Falletti, and L. L. Presti, "Performance comparison of a KF-based and a KF+VDFLL vector tracking-loop in case of GNSS partial outage and low-dynamic conditions," in *7th ESA Workshop on Satellite Navigation Technologies (NAVITEC)*, ESTEC, Noordwijk, The Netherlands, 2014, pp. 1-8.

[39] B. Xu and L.-T. Hsu, "Open-source matlab code for GPS vector tracking on a software-defined receiver," *GPS Solutions,* vol. 23, no. 2, 2019.

[40] Y. Luo, Y. Wang, S. Wu, and P. Wang, "Multipath effects on vector tracking algorithm for GNSS signal," *Science China Information Sciences,* vol. 57, no. 10, pp. 1-13, 2014.

[41] E. Amani, J.-R. de Boer, W. Vigneau, K. Djouani, and A. Kurien, "GPS multipath induced errors for the vector tracking loop: Insight into multipath detection," in *2016 European Navigation Conference (ENC 2016)*, Helsinki, Finland, 2016.

[42] E. Amani, K. Djouani, A. Kurien, J.-R. de Boer, W. Vigneau, and L. Ries, "GPS multipath detection in the frequency domain," in *2016 European Navigation Conference (ENC 2016)*, Helsinki, Finland, 2016.

[43] S. F. S. Dardin, V. Calmettes, B. Priot, and J.-Y. Tourneret, "Design of an adaptive vector-tracking loop for reliable positioning in harsh environment," in *Proceedings of the 26th International Technical Meeting of the ION Satellite Division (ION GNSS+2013)*, Nashville, Tennessee, 2013, pp. 3548-3559.

[44] E. D. Kaplan and C. J. Hegarty, *Understanding* GPS*: Principles and applications*. Boston: Artech House, 2006.

[45] Z. Sun, X. Wang, S. Feng, H. Che, and J. Zhang, "Design of an adaptive GPS vector tracking loop with the detection and isolation of contaminated channels," *GPS Solutions,* vol. 21, no. 2, pp. 701-713, 2016.

[46] J. B.-Y. Tsui, *Fundamentals of global positioning system receivers a software approach*, second edition ed. (Wiley series in microwave and optical engineering). Hoboken, New Jersey: John Wiley & Sons, Inc., 2005.

[47] D. H. Won *et al.*, "Weighted DOP with consideration on elevation-dependent range errors of gnss satellites," *IEEE Transactions on Instrumentation and Measurement,* vol. 61, no. 12, pp. 3241-3250, 2012.

[48] T. Suzuki. (2019, August 1). *GNSS radar*. Available: http://www.taroz.net/GNSS-Radar.html

[49] J. Xu, Q. Jia, Y. Luo, and L.-T. Hsu, "Intelligent GPS L1 LOS/multipath/NLOS classifiers based on correlator-, rinex- and nmea-level measurements," *Remote Sensing,* vol. 11, no. 16, 2019.

[50] E. Schmidt, Z. Ruble, D. Akopian, and D. J. Pack, "Software-defined radio GNSS instrumentation for spoofing mitigation: A review and a case study," *IEEE Transactions on Instrumentation and Measurement,* vol. 68, no. 8, pp. 2768-2784, 2019.

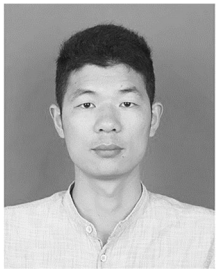

Bing Xu is currently a Postdoctoral Fellow with Interdisciplinary Division of Aeronautical and Aviation Engineering, The Hong Kong Polytechnic University. He received his B.S. and PhD. degrees in Network Engineering and Navigation Guidance and Control from Nanjing University of Science and Technology, China, in 2012 and 2018, respectively. His research focuses on signal processing in software defined GNSS receivers.

Qiongqiong Jia received her B.Sc. in Communication and Information Systems and M.Sc. in Communications Engineering from the Civil Aviation University of China in 2008 and 2011, respectively. She also received an advanced master degree in Air Navigation Engineering from École Nationale de l'Aviation Civil in France in 2015.

She is an associate professor of the Tianjin Key Laboratory for Advanced Signal Processing, Civil Aviation University of China. She is currently a research associate with the Interdisciplinary Division of Aeronautical and Aviation Engineering (AAE), the Hong Kong Polytechnic University. Her research interests include adaptive signal processing for multipath, NLOS and interference mitigation in GNSS.

Li-Ta Hsu (S'09–M'15) received the B.S. and Ph.D. degrees in aeronautics and astronautics from National Cheng Kung University, Tainan, Taiwan, in 2007 and 2013, respectively.

He is currently an assistant professor with Interdisciplinary Division of Aeronautical and Aviation Engineering, The Hong Kong Polytechnic University, Hong Kong, before he served as post-doctoral researcher in Institute of Industrial Science at The University of Tokyo, Tokyo, Japan. In 2012, he was a visiting scholar with the Faculty of Engineering, University College London, U.K. He is an associate fellow in royal institute of navigation (RIN) and a council member of institute of navigation (ION) since 2019. His research interests include His research interests include GNSS positioning in challenging environments and localization for autonomous driving vehicle and unmanned aerial vehicle.